International Journal of Heat and Mass Transfer 183 (2022) 122121

Contents lists available at ScienceDirect

International Journal of Heat and Mass Transfer

journal homepage: www.elsevier.com/locate/hmt

Modeling transpiration in synthetic trees

Ndidi L. Eyegheleme, Kurt Peng, Jonathan B. Boreyko*

Department of Mechanical Engineering, Virginia Tech, Blacksburg VA 24061, USA

ARTICLE INFO

Article history:
Received 2 August 2021
Revised 14 October 2021
Accepted 16 October 2021

Keywords:
Synthetic trees
Transpiration
Capillary-driven flow
Laplace pressure
Kelvin pressure

ABSTRACT

Synthetic trees mimic the transpiration cycle of natural trees by connecting a reservoir and conduits to wetted nanopores that exhibit a negative Laplace pressure during evaporation. Here, we develop a comprehensive theoretical model of transpiration for synthetic trees comprised of a vertically-oriented tube array connected at the top to a nanoporous synthetic leaf. Our model illustrates that when the leaf is exposed to a convective gas flow, the diffusive boundary layer is negligible and the ambient humidity directly prescribes the negative Laplace pressure of water in the leaf. The resulting capillary-driven transpiration rate up the tree is then a function of both the Laplace pressure, which sets the hydraulic load, and the tree geometry, which sets the hydraulic resistance. Conversely, when the leaf is exposed to an atmospheric environment, it is the evaporation rate and tree geometry that prescribe the necessary Laplace pressure to conserve mass. Matching the Laplace and Kelvin pressures at the menisci results in a local humidity that differs from the ambient, such that a diffusive boundary layer necessarily forms. Our model also accounts for the dynamic evolution of the menisci, in particular their ability to tune their contact angle and, when necessary, partially retreat into the nanopores to self-stabilize. Over a wide variety of tree geometries and ambient conditions, we identify when the transpiration rate is evaporation-limited versus pressure-limited (bottlenecked by the leaf's maximum Laplace pressure). These findings should inform the design and development of next-generation synthetic trees with applications in water extraction and solar steam generation.

1. Introduction

Trees spontaneously exert a hydraulic load to pump water into their roots, up xylem channels, and into their leaves to replace water lost by evaporation. This transpiration process is possible by holding the tree's water in tension (i.e. negative pressure), which is the result of evaporation causing a discrepancy in water activity between the leaf's saturated liquid and the air's subsaturated water vapor [1–7]. According to cohesion-tension theory, even an absolute negative water pressure is thermodynamically metastable (in the absence of vapor embryos), enabling a stable hydraulic load between the negative-pressure leaves and atmospheric water supply [8–16].

Scientists have taken inspiration from the transpiration process in nature to construct synthetic trees. The earliest report of a synthetic tree was in 1895, where Dixon and Joly steadily pumped water up a tube connected to porous cups on either end [17]. In 1928, Thut showed that a synthetic tree pre-filled with water could lift a bath of mercury up the tube as the water evaporates [18]. The ability to sustain an absolute negative water pressure was first demonstrated in 1970, where Hayward used a suction pump (rather than transpiration) to sustain a liquid column to a height of 17 m above its ambient reservoir [19]. While this report was not technically a synthetic tree, it nonetheless confirmed that the magnitude of the negative pressure can exceed that of the atmosphere. Using advanced nano/micro-fabrication to construct a tree-on-a-chip, Wheeler and Stroock showed in 2008 that a synthetic tree can sustain negative water pressures on the order of megapascals [20].

Recently, a series of reports by Noblin et al. and Stroock et al. exposed the synthetic leaf to a fixed partial pressure of water vapor using a convective air stream [3,20–23]. By passing the air stream through a flow meter and dew point generator, the desired partial pressure could be widely varied. The strong convection of this subsaturated air stream effectively collapsed the diffusive boundary layer to a negligible thickness. As a result, the ambient humidity was approximately equivalent to the local humidity immediately above the water menisci. This was confirmed by directly measuring the negative Laplace pressure (P_L) of the synthetic tree's water with a microtensiometer, equating it to the Kelvin pressure (P_k), and solving the Kelvin equation for the local humidity which was roughly equivalent to that of the ambient [24]. Remarkably, beneath the critical humidity where the resulting

* Corresponding author.
E-mail address: boreyko@vt.edu (J.B. Boreyko).

https://doi.org/10.1016/j.ijheatmasstransfer.2021.122121
0017-9310/

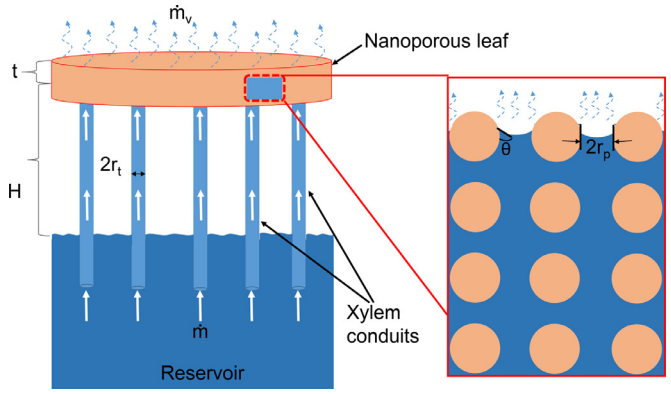

Fig. 1. Schematic of a model synthetic tree system. The tree is comprised of a vertical array of conduits, where the top ends are interfaced with a nanoporous disk and the bottom ends with a bulk reservoir of water. Inset shows the concavity of the menisci within the nanopores during evaporation, from which a negative Laplace pressure is generated and transmitted across the tree as a hydraulic load.

Kelvin stress exceeds the maximum possible negative Laplace pressure ($P_{L,max}$, where the menisci exhibit the receding contact angle, θ_R), the menisci are able to self-stabilize by partially retreating into the nanopores to increase their local humidity [25]. In this special case, there is now a concentration boundary layer within the receded nanopores, but still none above the leaf.

Conversely, many other synthetic trees expose the synthetic leaf to an ambient environment of subsaturated air [26–30]. In this case, the concentration boundary layer across which diffusion occurs is now significant. The local humidity is now higher than that of the ambient, such that the Kelvin and Laplace pressures acting at the menisci are not known a priori. A recent report showed that the Kelvin and Laplace pressures, and by extension the local humidity, could be estimated by measuring the transpiration rate and invoking conservation of mass for a tree with a known hydraulic resistance [31].

In summary, it is now evident that synthetic trees are far from monolithic in terms of what governs their transpiration rate and negative water pressure. These parameters depend on whether convection is present above the leaf, the water activity of the air, the pore radius and thickness of the synthetic leaf, and the number and dimensions of the conduits that connect the leaf to the water supply. To the best of our knowledge, there has not been any comprehensive work that rationalizes the flow rate and water pressure of synthetic trees for any possible combination of these parameters. Here, we clarify the order of operations for how to model the transpiration dynamics of a synthetic tree for any given ambient condition and tree geometry. Our model captures the crossover between an evaporation-limited regime, where the transpiration rate varies depending on the environmental/thermal conditions, and a pressure-limited regime, where the transpiration rate plateaus to a maximal value dependent upon the tree geometry. In particular, our model reveals that maximizing the Laplace suction does not optimize the transpiration rate for most tree designs, as the small nanopores required cause a non-linear increase in the viscous pressure drop across the leaf.

2. Model formulation

The model tree considered in this report is comprised of a parallel array of vertical tubes, whose upper ends are embedded within a thin, horizontally-oriented nanoporous disk as depicted in Fig. 1. The inner radius of each tube was fixed at $r_t = 1.59$ mm and the number of tubes was fixed at $N = 19$, consistent with the tubes used in recent reports that experimentally validated the concept of a scalable synthetic tree [31,32]. The vertical height of the tube array, spanning from the free surface of the lower reservoir to the nanoporous leaf, was varied as either $H =$ 10 m, 100 m, or 1,000 m. The cross-sectional area of the nanoporous disk (i.e. leaf) was fixed as $A = 2.29 \times 10^{-3}$ m^2, while the disk thickness was either $t = 1$ μm or 10 μm (aside from select graphs where t was varied continuously). The effective nanopore radius of the disk, when not varied continuously, was either $r_p = 1$ nm, 10 nm, or 100 nm. The porosity and tortuosity of the nanopores were fixed to $\Phi = 0.32$ and $\tau = 3.5$, respectively, again in consonance with recent experimental reports [31,32]. This resulted in a permeability of $k = 1.28 \times 10^{-17}$ m^2/Pa·s, 1.28×10^{-15} m^2/Pa·s, and 1.28×10^{-13} m^2/Pa·s, respectively, for the aforementioned three choices in r_p. The receding contact angle of the water menisci within the nanoporous leaf was fixed to $\theta_R = 0^\circ$ for some graphs, and varied continuously from 0° to 90° for others.

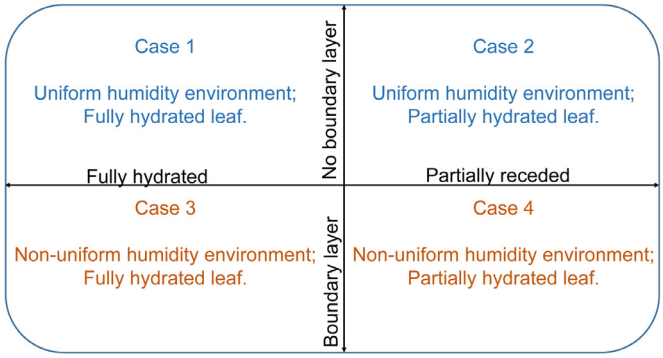

Fig. 2. Diagram that summarizes the four different modes of operation for synthetic trees.

This model tree system was analyzed for two different environmental conditions: a uniform humidity environment, where a convective gas flow collapses the diffusive boundary layer, and an ambient environment, where the far-field humidity is smaller than the local humidity directly above the menisci. For each environmental condition there are in turn two sub-regimes: either the menisci remain at the top of the nanoporous leaf, or they partially recede due to the required Laplace suction exceeding its maximum possible value. Therefore, four total cases are possible, as summarized in Fig. 2.

3. Results and Discussion

Uniform Humidity Environment.

In this first section, we will only consider a uniform humidity environment, where the diffusive boundary layer above the synthetic leaf is negligibly thin. This corresponds to Cases 1 and 2 in Fig. 2 and is shown visually in Fig. 3. The stress acting on the menisci within the leaf's nanopores is due to the mismatch in chemical potential between the saturated water and subsaturated vapor. This stress is quantified by the Kelvin pressure equation [20,33]:

$$P_K = \frac{RT}{\nu}\ln(a_l), \tag{1}$$

where R is the universal gas constant, T is the temperature at the liquid-vapor interface, ν is the liquid molar volume, and a_l is the local water activity directly above the meniscus. The water activity itself is defined as the ratio of the partial pressure of water vapor to the saturation pressure of water at the same temperature: $a = p_{vap}/p_{sat}$. For a uniform humidity environment, the local water activity is approximately equal to that of the ambient: $a_l \approx a_\infty$, where a_∞ is easily measured by a hygrometer.

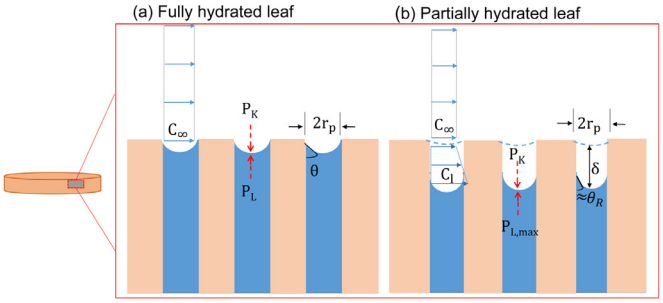

Fig. 3. Schematic of a synthetic leaf in a pure vapor environment, where the concentration field above the leaf is uniform (i.e. negligible boundary layer). (a) When the Kelvin pressure imposed on the menisci by the subsaturated ambient is less than the maximum possible Laplace pressure ($|P_K| = |P_L| < |P_{L,max}|$), the menisci are stabilized along the outer face of the synthetic leaf (i.e. full hydration). (b) When the ambient Kelvin stress exceeds the maximum possible Laplace pressure ($|P_K| > |P_{L,max}|$), the menisci recede until achieving an increased local vapor concentration (c_l) where $P_K \approx P_{L,max}$.

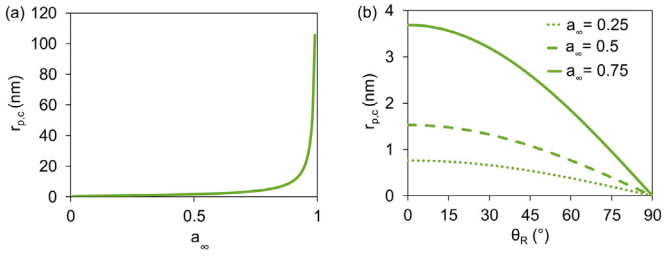

Fig. 4. Plots of the critical pore radius, above which crossover from the evaporation-limited regime to the pressure-limited regime occurs. (a) The critical pore radius is graphed as a function of the ambient water activity, calculated from Eq. 1 and Eq. 4 for a range of water activities ($a_\infty = 0.1$–1.0) and assuming room temperature conditions ($T = 25$ °C). (b) The critical pore radius is now graphed against the receding contact angle, calculated from Eqs. 1 and 4 with $|P_K| = 190.3$ MPa, 95.1 MPa, and 39.5 MPa corresponding to 25%, 50%, and 75% relative humidities, respectively.

To achieve physical equilibrium (i.e. avoid dryout), the Kelvin pressure must be balanced by the Laplace pressure. The concave curvature of the menisci within the nanopores generates a negative Laplace pressure: [3]

$$P_L = -\frac{2\gamma\cos\theta}{r_p}, \tag{2}$$

where γ is the surface tension of water, θ is the contact angle of the meniscus with respect to the side walls of the nanopores, and r_p is the average pore radius. The Kelvin-Laplace relation predicts the condition for meniscus stability as $P_K = P_L$, which for a given local humidity and pore size predicts the value of θ at equilibrium [20,23,25,34].

This Laplace pressure also represents the total pressure differential across the synthetic tree, extending from the upper leaf to the lower reservoir of water of atmospheric pressure. In other words, the negative Laplace pressure (P_L) is balanced by the positive pressure drops across the tree (ΔP). The total pressure drop is the sum of the viscous pressure drop across the nanoporous leaf, the viscous pressure drop in the tubes, and the hydrostatic pressure in the tubes. The pressure drop across the leaf is evaluated using Darcy's law: $\Delta P_D = (Qt)/(kA)$, [25,35] with Q being the volumetric flow rate, t and A are the thickness and cross-sectional area of the leaf, and $k = (\Phi r_p^2)/(8\mu\tau)$ is the permeability of the nanopores, where Φ is the disk porosity, μ is the liquid water viscosity, and τ is the tortuosity [36,37]. The viscous pressure drop in the tubes is evaluated using Poiseuille's equation, [20,38] $\Delta P_P = (8QH\mu)/(\pi N r_t^4)$, with H being the height of the tubes, r_t the radius of tubes, and N the total number of tubes in the array. The hydrostatic pressure drop in the tubes is $\Delta P_G = \rho g H$, where ρ is the density of liquid water. Balancing the Laplace pressure against the pressure drops:

$$|P_L| = \Delta P = \Delta P_D + \Delta P_P + \Delta P_G. \tag{3}$$

For a synthetic leaf where r_p is known and $a_\infty \approx a_l$ is controlled, Eqs. 1 and 2 can be combined to solve for $|P_L|$. In turn, plugging $|P_L|$ into Eq. 3 allows for the solution of the volumetric transpiration rate (Q). It is trivial to then extract the liquid mass flow rate as $\dot{m} = \rho Q$. By conservation of mass, the liquid mass flow rate up the tree is equivalent to the evaporation mass flow rate from the leaf, $\dot{m} = \dot{m}_v$, during steady-state operation.

The maximum possible Laplace pressure, as defined earlier, corresponds to when the contact angle of the menisci reaches its minimum value:

$$P_{L,\,max} = -\frac{2\gamma\cos\theta_R}{r_p}, \tag{4}$$

where θ_R is the receding contact angle of the menisci. When $P_K = P_L$ is satisfied for a contact angle exceeding the receding contact angle ($\theta > \theta_R$), the menisci are stable and the entire leaf remains wetted. In Fig. 2, this case of a uniform humidity environment with fully hydrated nanopores is referred to as Case 1. However, when the imposed relative humidity results in $|P_K| > |P_{L,\,max}|$, equilibrium is not possible and the menisci retreat into the nanopores (Case 2).

As the menisci retreat, the local humidity increases due to the choking of water vapor within the dried-out nanopores, i.e. now $a_l > a_\infty$ which decreases P_K (Fig. 3b) [25,30]. The menisci therefore halt their retreat once the local humidification satisfies $P_K = P_{L,\,max}$. The critical retreat distance, δ, where equilibrium occurs can be estimated by: [25]

$$\frac{\delta}{t-\delta} = \frac{P_{L,max} - P_K}{-P_{L,max}} \times \beta, \tag{5}$$

where $\beta = g_{vap}/g_{liq}$ is the ratio of conductance of the vapor to that of the liquid. Similar to Case 1, Eq. 3 can be solved for the transpiration rate, but now $P_{L,\,max}$ is plugged into the left-hand side. Case 2 therefore corresponds to the maximum possible transpiration rate for a given tree geometry, as $P_{L,\,max}$ represents the maximal hydraulic load across the tree. For this reason, the volumetric and mass flow rates for Case 2 will be referred to as Q_{max} and $\dot{m}_{max}$, respectively. Case 1 is an evaporation-limited regime, where the transpiration rate increases monotonically with decreasing a_∞. Conversely, Case 2 is a pressure-limited regime, where the transpiration rate is fixed by the maximum Laplace pressure regardless of the value of a_∞.

Fig. 4 (a) shows the relationship between the critical pore radius and the ambient water activity. This critical pore radius, $r_{p,c}$, is the pore size for a given a_∞ where $P_K = P_{L,\,max}$ and $\theta = \theta_R$ for the first time. In other words, $r_p < r_{p,c}$ corresponds to the evaporation-limited regime (Case 1), where the leaf is fully hydrated and $\theta > \theta_R$, whereas $r_p > r_{p,c}$ corresponds to the pressure-limited regime (Case 2), where the menisci have partially retreated and the transpiration rate is maximal. The values of $r_{p,c}$ were obtained by plugging a given value of $a_\infty \approx a_l$ into Eq. 1, equating with Eq. 4, and solving for $r_p = r_{p,c}$ with $\theta_R \approx 0°$ (i.e. assuming superhydrophilic leaf pores). From the curve, it can be seen that the critical pore size increases as the ambient water activity is increased. This is because a higher water activity will impose a lower external thermodynamic pressure against the meniscus, such that a smaller magnitude Laplace pressure (and by extension a larger pore size) is needed to maintain stability. For instance, an ultra-dry humidity of $a_\infty \approx a_l = 0.1$ will impose an immense Kelvin pressure of $|P_K| = 316$ MPa, requiring $r_{p,c} = 0.46$ nm or less to maintain full leaf hydration (Case 1). In contrast, increasing the water activity

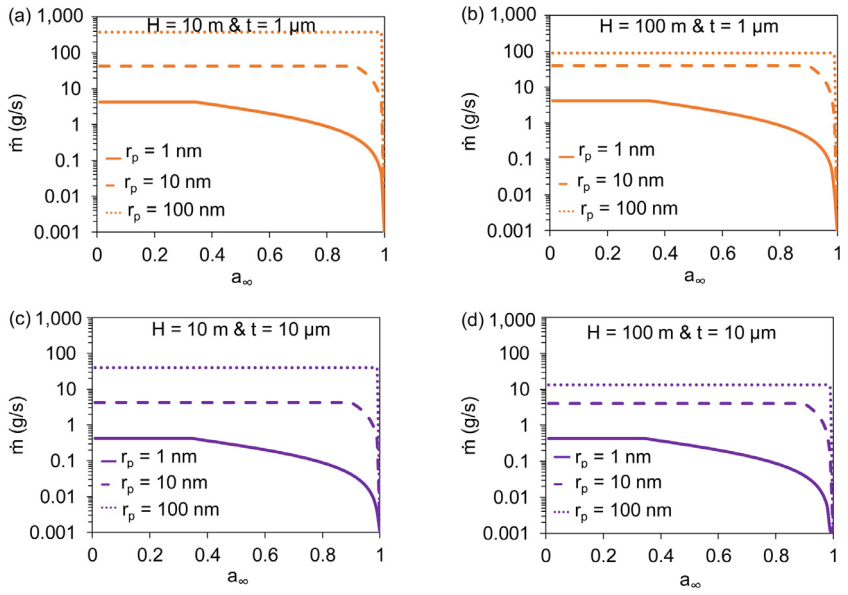

Fig. 5. Graphs of the transpiration mass flow rate versus ambient water activity. The transpiration rate is calculated from a_∞ and the given tree geometry using Eqs. 1,2, and 3. The transition from the pressure-limited regime to the evaporation-limited regime occurs when the value for $\dot{m}$ is no longer constant with increasing a_∞. Three choices for the effective radius of the leaf's nanopores are used in all graphs, while the tube height and leaf thickness are varied as (a) $H = 1$ m and $t = 1$ μm, (b) $H = 100$ m and $t = 1$ μm, (c) is $H = 10$ m and $t = 10$ μm, and (d) $H = 100$ m and $t = 10$ μm.

by a factor of four to $a_\infty \approx a_l = 0.4$ imposes $|P_K| = 125.7$ MPa on the meniscus, which increases the critical pore radius by a factor of 2.5 ($r_{p,c} = 1.16$ nm). Around $a_\infty \approx a_l = 0.9$, the value of $r_{p,c}$ rapidly increases due to the asymptotic limit of an infinite critical pore size at 100% humidity.

Fig. 4(b) shows how the critical nanopore radius varies with changing receding contact angle for three ambient water activity values: $a_\infty = 0.25$, 0.5, or 0.75. The curve shows that increasing the water activity from 0.25 to 0.5 roughly doubles $r_{p,c}$, but a subsequent increase of the water activity to 0.75 causes a much larger (non-linear) increase in $r_{p,c}$. It can also be observed that increasing θ_R, which in turn decreases $|P_{L,\,max}|$, requires increasingly small values of $r_{p,c}$. This is because for a higher receding angle, the concave meniscus cannot achieve as small of a radius of curvature for a given pore size, effectively decreasing the maximum achievable Laplace pressure prior to meniscus retreat. For all three imposed water activities, increasing the receding contact angle by a factor of four, from 15° to 60°, roughly halves the critical pore size.

Fig. 5 depicts how the transpiration rate changes with the imposed water activity for 12 different tree geometries. For Case 1, the values of $\dot{m}$ were calculated by combining Eqs. 1–3, whereas Eqs. 3–4 were used to calculate the plateau value of $\dot{m}_{max}$ for Case 2. As expected, the transpiration rate decreases with increasing a_∞, as an increasingly lower Kelvin pressure is exerted at the meniscus which by extension reduces the required suction pressure ($|P_L|$). The crossover between Case 1 and Case 2, i.e. the onset of $\dot{m}_{max}$, occurs at much lower values of a_∞ for smaller nanopore sizes. Conversely, although leaves with larger nanopores plateau to a maximum transpiration rate much sooner with decreasing humidity, resulting in a lower $|P_{L,\,max}|$, counter-intuitively the resulting $\dot{m}_{max}$ is larger by 1–2 orders of magnitude. This is because the influence of r_p on the Darcy pressure drop across the nanoporous leaf ($\Delta P_D \propto r_p^{-2}$) out-competes the corresponding change in the suction pressure ($|\Delta P_L| \propto r_p^{-1}$).

Taking the $H = 10$ m tall tree with a leaf thickness of $t = 1$ μm as an example (Fig. 5a), the smallest pore radius of $r_p = 1$ nm can remain in the evaporation-limited regime (Case 1) until dropping to a water activity of $a_\infty \approx 0.35$. In contrast, a moderate pore size of $r_p = 10$ nm can only sustain Case 1 down to $a_\infty \approx 0.9$, while the largest nanopores, $r_p = 100$ nm, reach an extremely early plateau at $a_\infty \approx 0.99$. This illustrates how synthetic trees with sufficiently small nanopores can result in a wide variety of possible transpiration rates, depending on the external humidity, whereas trees with large nanopores can exhibit an essentially fixed flow rate regardless of the environmental conditions. The immense hydraulic resistance of the leaf with $r_p = 1$ nm results in a maximum transpiration rate of only $\dot{m}_{max} \sim 1$ g/s, compared to $\dot{m}_{max} \sim 10$ g/s for $r_p = 10$ nm and $\dot{m}_{max} \sim 100$ g/s for $r_p = 100$ nm.

In Fig. 5b, the tree height is increased an order of magnitude to $H = 100$ m. This increases the hydrostatic pressure drop by an order of magnitude, which reduces the portion of $|P_L|$ which can be devoted to overcoming the Darcy pressure in the leaf. As a consequence, the transpiration rate decreases for any given value of a_∞. The magnitude of the decrease in $\dot{m}$ is dramatic for the largest pore size, because the maximum suction of $|P_{L,max}| = 1.46$ MPa is almost entirely consumed by gravity ($P_G \approx 1$ MPa), leaving little left for viscous flow. As a consequence, the maximum transpiration rate drops by nearly an order of magnitude. In contrast, for the smallest pore size $|P_{L,max}| = 146$ MPa, such that the viscous flow rate is barely affected by the comparatively minute increase in the hydrostatic load.

Comparing the graphs in Fig. 5(a,c) or Fig. 5(b,d), the leaf thickness is now increased by an order of magnitude to $t = 10$ μm. Given the aforementioned predominance of the Darcy pressure drop in most cases, this increase in t results in a dramatic decrease in $\dot{m}$. For cases where the hydrostatic pressure drop is minimal compared to $|P_{L,max}|$ (ex: $r_p = 10$ nm), the decrease in $\dot{m}$ is by almost exactly an order of magnitude, corresponding to the increase in P_D by one order. Conversely, when the hydrostatic load is dominant, as with $r_p = 100$ nm and $H = 100$ m, the decrease in $\dot{m}$ is only by about half an order of magnitude.

Fig. 6 shows how varying the nanopore radius can affect both the maximum transpiration rate (left y-axis) and the maximum Laplace pressure (right y-axis). Increasing the pore size results in a non-linear increase in leaf permeability, such that $\dot{m}_{max}$ increases due to the dramatic decrease in P_D relative to the weaker increase in suction. The shape of the curve of $\dot{m}_{max}$ versus r_p is the same shape for all three choices of leaf thickness, with the magnitude

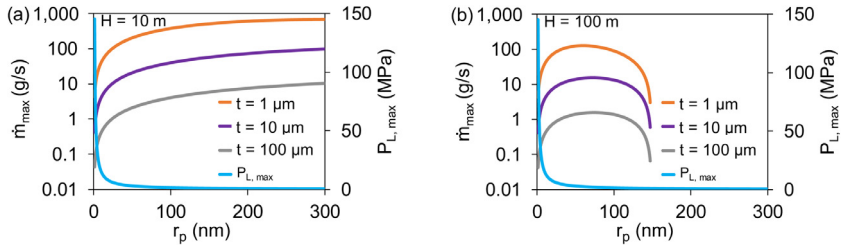

Fig. 6. Graphs of the maximum possible transpiration rate (left y-axis) and Laplace pressure (right y-axis), as functions of the nanopore radius. The maximum Laplace pressure was calculated using Eq. 4 with $\theta_R = 0^\circ$, while $\dot{m}_{max}$ was then calculated from Eq. 3. Both graphs have three choices for the leaf thickness and the height of the tree was either (a) $H = 10$ m or (b) $H = 100$ m.

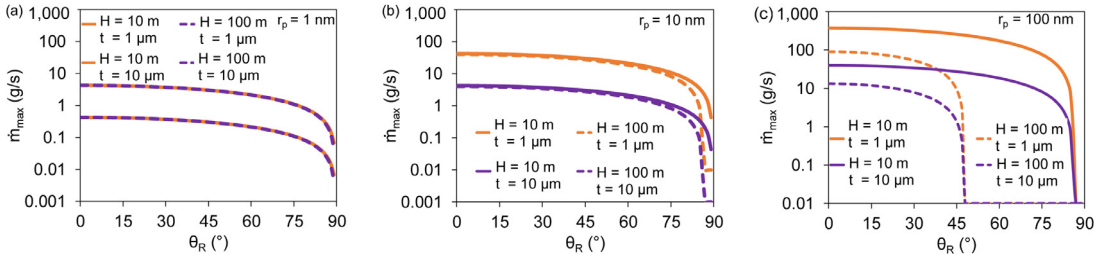

Fig. 7. Plots of the maximum possible transpiration rate versus the receding contact angle of the nanoporous leaf. First, $P_{L,max}$ was calculated from Eq. 4 for each value of θ_R, and subsequently $\dot{m}_{max}$ was found using Eq. 3. All three graphs employ the same four combinations of tree height ($H = 10$ or 100 m) and leaf thickness ($t = 1$ or 10 μm), while the nanopore size is fixed as (a) $r_p = 1$ nm, (b) $r_p = 10$ nm, or (c) $r_p = 100$ nm.

increasing with decreasing t. The relationship of $|P_{L,max}|$ versus r_p is the exact opposite (i.e. decreasing with increasing pore size), as shown in Eq. 4.

When increasing the tree height to $H = 100$ m (Fig. 6b), the $\dot{m}_{max}$ curves are initially the same for small values of r_p. This is because the Darcy pressure dominates over the hydrostatic pressure for very small nanopores, as previously discussed. For instance, at a pore radius of $r_p = 2$ nm, the Darcy pressure is at least six orders of magnitude larger than the hydrostatic pressure for any given leaf thickness. For larger pores, the Darcy pressure drop becomes smaller relative to the hydrostatic pressure. Above a critical nanopore radius where $|P_{L,max}| = P_G$, the water columns in the synthetic tree can no longer be sustained against gravity. For the tree height of 100 m, this occurs for all three leaf thicknesses at a critical pore radius of about $r_{p,c} \approx 150$ nm.

Fig. 7 depicts how the maximum transpiration rate can be tuned by changing the receding contact angle for different tree geometries. Smaller values of θ_R increase the maximum Laplace pressures (Eq. 4), because the menisci can achieve a smaller radius of curvature before retreating into the nanopores. This larger possible suction pressure translates to a higher maximum transpiration rate, by increasing the value of Q that satisfies Eq. 3.

Fig. 7 (a) shows that for very small nanopores ($r_p = 1$ nm), the maximal transpiration rate increases by about two orders of magnitude when decreasing θ_R from 89° down to 0°. For any given value of θ_R, increasing the leaf thickness from $t = 1$ μm to $t = 10$ μm serves to decrease $\dot{m}_{max}$ by an order of magnitude. This is due to the viscous losses in the leaf (i.e. Darcy pressure) being the dominant pressure drop in the tree when using small nanopores. In contrast, varying the tree height between $H = 10$ m and 100 m did not appreciably change the curves for $\dot{m}_{max}$ versus θ_R.

Fig. 7 (b) shows that for medium sized nanopores ($r_p = 10$ nm), the tree height begins to affect $\dot{m}_{max}$ but only at larger receding angles ($\theta_R > 70^\circ$). This is because, at these large angles, the corresponding value of $P_{L,max}$ is approaching the magnitude of the hydrostatic pressure in the tubes. As a consequence, there is very little suction available to overcome the viscous losses in the leaf, resulting in the plummeting values of $\dot{m}_{max}$ for the case of a tall tree ($H = 100$ m). For lower values of θ_R, the curves look qualitatively similar to those in Fig. 7(a), but shifted an order of magnitude higher due to the larger nanopore size reducing the Darcy pressure.

In the extreme case of having very large nanopores ($r_p = 100$ nm), both the tree height and leaf thickness modify the $\dot{m}_{max}$ curves even for small values of θ_R. This is because of the dramatic reduction in the Darcy pressure drop for such large nanopores, such that the Darcy and hydrostatic pressure drops are of comparable magnitude. For example, increasing the tree height by an order of magnitude causes a three-fold reduction in $\dot{m}_{max}$, while increasing the leaf thickness by an order of magnitude causes $\dot{m}_{max}$ to decrease by nearly an order of magnitude. As the receding contact angle is increased beyond a critical value, the hydrostatic pressure consumes all of the Laplace pressure and the flow rate vanishes. This occurs around $\theta_R = 87^\circ$ for the $H = 10$ m tree and around $\theta_R = 48^\circ$ for the $H = 100$ m tree.

Fig. 8 shows how the maximum transpiration rate and meniscus retreat distance changes as the leaf thickness is changed, given a fixed ambient humidity of 50%. Under such dry conditions, the Kelvin stress corresponding to the ambient humidity always exceeds the maximum possible Laplace pressure for the cases of $r_p = 10$ nm (Fig. 8a) and $r_p = 100$ nm (Fig. 8b). Therefore, the menisci are forced to retreat within the nanopores until achieving a local humidity within the dried-out nanopores that reduces P_K to match $P_{L,max}$, enabling stable transpiration at the maximum possible flow rate ($\dot{m}_{max}$).

The maximum transpiration rate (left y-axis) decreases exponentially with increasing disk thickness, due to the increase in the Darcy pressure drop. Fig. 8(a) shows that for smaller nanopores, increasing the height of the tree from $H = 10$ m to 100 m only decreases $\dot{m}_{max}$ by about 7%. This indicates that the viscous pressure drop across the leaf dominates the hydrostatic pressure drop across the tubes. For the larger nanopores in Fig. 8(b), however, the same increase in height substantively lowered $\dot{m}_{max}$ by a factor of 2.5–4.2 (depending on the value of t). This is due to the smaller Darcy pressure becoming comparable to the hydrostatic pressure.

From the relationship given in Eq. 5, the critical retreat distance into the nanopores (right y-axis) increases linearly with t. The con-

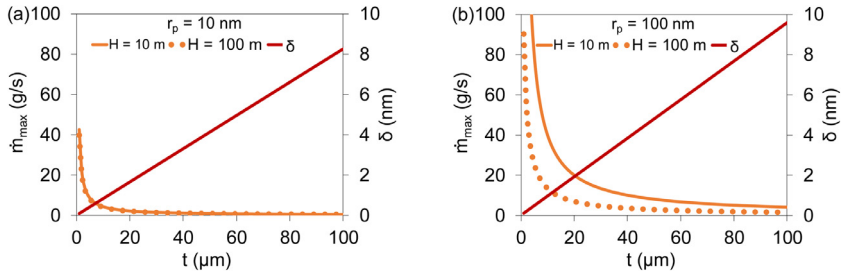

Fig. 8. The maximum transpiration rate (left y-axis), as well as the retreat distance required to stabilize the menisci (right y-axis), can be tuned by changing the leaf thickness. Values for $\dot{m}_{max}$ were calculated with Eq. 4 (using $\theta_R = 0$ °C) combined with Eq. 3. Curves for δ were generated using Eq. 1 for a fixed ambient humidity of 50%, resulting in $|P_k| = 95.1$ MPa, combined with Eq. 5. (a) When $r_p = 10$ nm, $|P_{L,max}| = 14.5$ MPa the leaf permeability is $k = 1.28 \times 10^{-15}$ m^2/Pa·s, and the linear conductance ratio is $\beta = 1.49 \times 10^{-5}$. (b) When $r_p = 100$ nm, $|P_{L,max}| = 1.45$ MPa, $k = 1.28 \times 10^{-13}$ m^2/Pa·s, and $\beta = 1.49 \times 10^{-6}$.

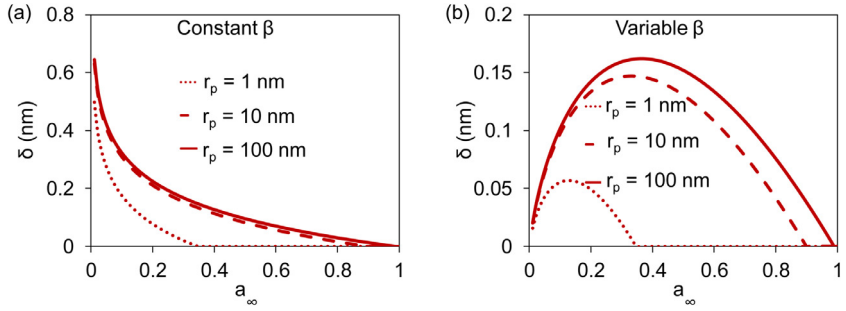

Fig. 9. The retreat distance as a function of the ambient water activity. Values for δ are calculated using Eqs. 1, 4 and 5. (a) The linear conductance ratio, β, was chosen to be independent of the changes in the external vapor pressure. It was calculated using Eq. 6 with a representative mean ambient vapor pressure of $p_{vap} = 1$ kPa to yield $\beta = 1.49 \times 10^{-4}$, 10^{-5}, or 10^{-6} for $r_p = 1$, 10, or 100 nm, respectively. (b) The linear conductance ratio was varied with a_∞. Specifically, $p_{vap} = a_\infty p_{sat}$ was plugged into Eq. 6 to obtain β.

ductance ratio is calculated from: [25]

$$\beta \approx \frac{32}{3}\left(\frac{2}{\pi}\right)^{1/2}\left(\frac{RT}{\nu\rho}\right)^{-3/2}\frac{\mu p_{vap}}{r_p \rho^2}. \quad (6)$$

Comparing $r_p = 10$ nm (Fig. 8a) with $r_p = 100$ nm (Fig. 8b), the magnitude of the retreat is larger for the latter by roughly 20%. This is due to the much smaller maximum Laplace pressure of the larger nanopores: $|P_{L,max}| = 1.45$ Mpa compared to $|P_{L,max}| = 14.5$ Mpa for the smaller nanopores. In turn, this means the larger nanopores also require a smaller local Kelvin stress above the menisci, such that a greater local humidity is required to achieve equilibrium. Quantitatively, the menisci retreat within the $r_p = 10$ nm leaf until reaching a local humidity of 89.97%, compared to the $r_p = 100$ nm leaf which must retreat to a 98.95% humidity. Considering the dramatic difference in local humidities, it is initially surprising that the retreat distance is only slightly increased for the $r_p = 100$ nm case. However, this is readily explained by the simultaneous change in the ratio of vapor conductance to liquid conductance, which is smaller for $r_p = 100$ nm. Overall, the retreat distances for a pure vapor environment are nanometric, such that very thin synthetic leaves can achieve equilibrium before drying out.

Fig. 9 shows how the retreat distance varies with the ambient humidity. In Fig. 9(a), the linear conductance ratio (β from Eq. 5) is approximated as being constant for a given value of r_p. This was done by calculating β at a mean external vapor pressure of 1 kPa, consistent with the approach used by Vincent et al. [25]. For all three pore sizes considered, the retreat distance decays exponentially with increasing ambient water activity. This is physically intuitive, as when β and the leaf geometry is fixed, the retreat distance solely depends on the Kelvin stress corresponding to the ambient humidity. A smaller value of a_∞ demands a longer retreat to achieve the local humidity where equilibrium is achieved. The retreat distance was by far the smallest for the smallest nanopores ($r_p = 1$ nm), whereas δ was only slightly smaller for $r_p = 10$ nm compared to $r_p = 100$ nm. Especially for the smaller pore sizes, above a critical value of a_∞ there is no longer any retreat, as the menisci are able to balance the Kelvin stress at a Laplace pressure less than the maximum value. In other words, when $\delta = 0$, the tree is operating in the evaporation-limited regime where the transpiration rate depends on a_∞, whereas when $\delta > 0$, the tree is in the pressure-limited regime at a fixed $\dot{m}_{max}$.

Considering the full range of values considered here for a_∞, it may be more physical to allow the linear conductance ratio to vary with the external vapor pressure. As seen in Fig. 9(b), this now results in a non-monotonic relationship, where counter-intuitively δ can now increase with increasing a_∞ for cases where the humidity is low. This is because a non-fixed β increases with a_∞, making it more difficult to choke the vapor within the dried-out nanopores to achieve local humidification. Over the low range of a_∞ values, this effect is actually out-competing the importance of the decrease in Kelvin stress that occurs with increasing a_∞, such that a larger retreat is required with increasing ambient humidity. At the peak of each curve, the change in Kelvin stress now becomes predominant over the variation in β, such that δ now lowers with increasing a_∞. This cross-over occurs at a relative humidity of 13% for $r_p = 1$ nm, 32% for $r_p = 10$ nm, and 36% for $r_p = 100$ nm. A second cross-over, from the evaporation-limited regime to the pressure-limited regime, occurs when δ reaches zero at an ambient humidity of 34% for $r_p = 1$ nm, 89% for $r_p = 10$ nm, and 98% for $r_p = 100$ nm.

The local water activity (i.e. local humidity) above the menisci are plotted in Fig. 10 as a function of the nanopore radius (left y-axis). For sufficiently small nanopore radii, the local water activity matches that of the ambient ($a_l = a_\infty$), as the maximum Laplace pressure exceeds the ambient Kelvin stress. Therefore, the menisci do not need to retreat, resulting in $\delta = 0$ (right y-axis). For this no-retreat condition, the equilibrium contact angle of the menisci can

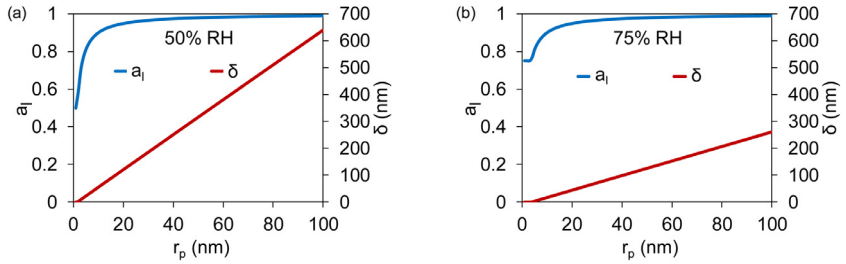

Fig. 10. The local water activity (left y-axis) and retreat distance (right y-axis) as functions of the nanopore radius. Values for a_l and δ are calculated using Eqs. 1, 4, 5, and 6. Tree properties include $\theta_R = 0$ °C and $t = 100$ μm. The ambient humidity was either (a) 50% ($|P_k| = 95.1$ MPa) or (b) 75% ($|P_k| = 39.5$ MPa).

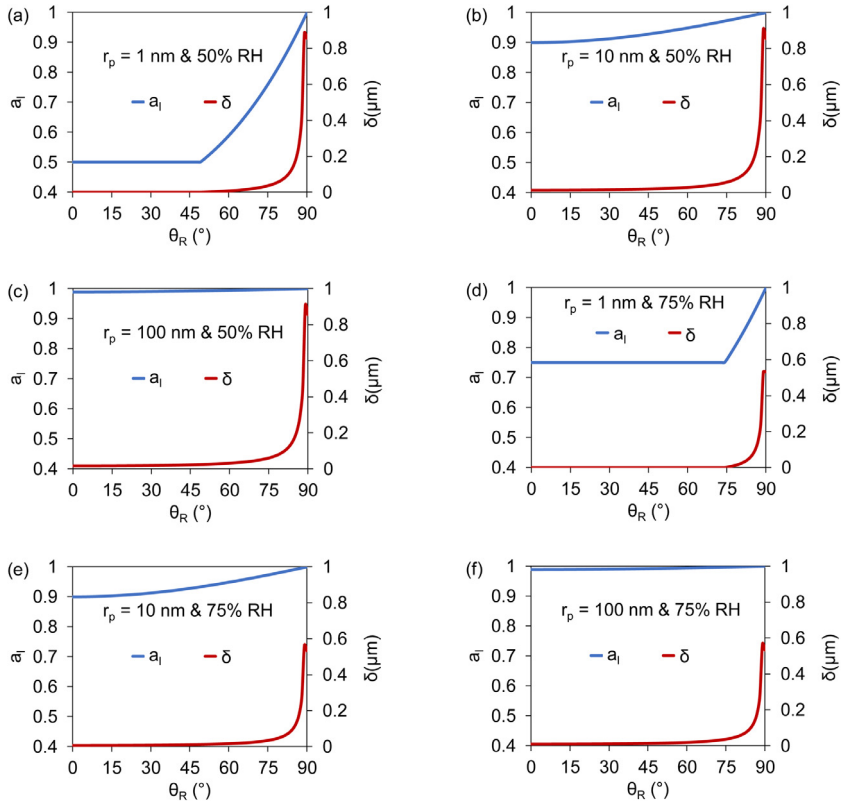

Fig. 11. The local water activity (left y-axis) and retreat distance (right y-axis) as functions of the receding contact angle. Values are calculated from Eqs. 1, 2, 4, 5, and 6 with $t = 100$ μm. (a–c) The ambient humidity was 50% with nanopore sizes of $r_p = 1$, 10, and 100 nm, respectively, resulting in $\beta = 2.36 \times 10^{-4}$, $\times 10^{-5}$, or $\times 10^{-6}$. (d–f) The ambient humidity was 75% with nanopore sizes of $r_p = 1$, 10, and 100 nm, respectively, resulting in $\beta = 3.54 \times 10^{-4}$, $\times 10^{-5}$, or $\times 10^{-6}$.

be solved if desired by equating Eq. 1 and Eq. 2, setting $a_l = a_\infty$, and solving for θ.

When the ambient humidity is 50% (Fig. 10a), retreat occurs for $r_p > 1.53$ nm, indicating that menisci retreat is required for all but the smallest nanopores. For a higher ambient humidity of 75% (Fig. 10b), retreat occurs above a larger critical nanopore size of $r_p > 3.69$ nm. When retreat occurs, the local humidity was solved by equating Eq. 1 and Eq. 4 (setting $\theta_R = 0°$). The retreat distance was then solved using Eq. 5 and assuming a constant vapor pressure for β. The retreat distance increases linearly with the nanopore radius, which is due to a combination of the non-linear increase in required local humidity and the dependence of β on r_p. The slope of δ versus r_p is about 2.4 times higher for the ambient humidity of 50% compared to 75%.

Fig. 11 depicts the same dependent variables of a_l and δ, but now plotted as a function of the nanopores' receding contact angle for three fixed nanopore radii of $r_p = 1$, 10, and 100 nm. For the smallest pore radius considered and sufficiently small values of θ_R, $a_l = a_\infty$ and $\delta = 0$. As with the previous figure, this is because over this parameter space the maximum Laplace pressure exceeds the ambient Kelvin stress, precluding the need for partial retreat. Retreat and local humidification begin above a critical receding contact angle of $\theta_R > 50°$ for a 50% ambient humidity (Fig. 11a) and for $\theta_R > 75°$ for a 75% ambient humidity (Fig. 11d). This exact numerical match of the critical θ_R and ambient humidity is coincidental, only occurring for this arbitrary choice of $r_p = 1$ nm. Increasing the pore radius to $r_p = 10$ nm (Fig. 11b,e) or $r_p = 100$ nm (Fig. 11c,f) requires the menisci to retreat over the entire range of θ_R values. This is because the maximum Laplace pressure that the pores can support is greatly reduced for larger nanopores, such that it is always less that the Kelvin stress corresponding to 50% or 75% humidity. As the 75% ambient humidity imposes a smaller Kelvin stress on the menisci, the magnitude of retreat is smaller compared to 50% humidity.

The local water activity, plotted as the second y-axis in Fig. 11, equals the ambient value when $\delta = 0$ and then increases with δ as the menisci retreat. This local water activity can be determined by equating Eq. 2 to Eq. 1 and plugging in the receding contact

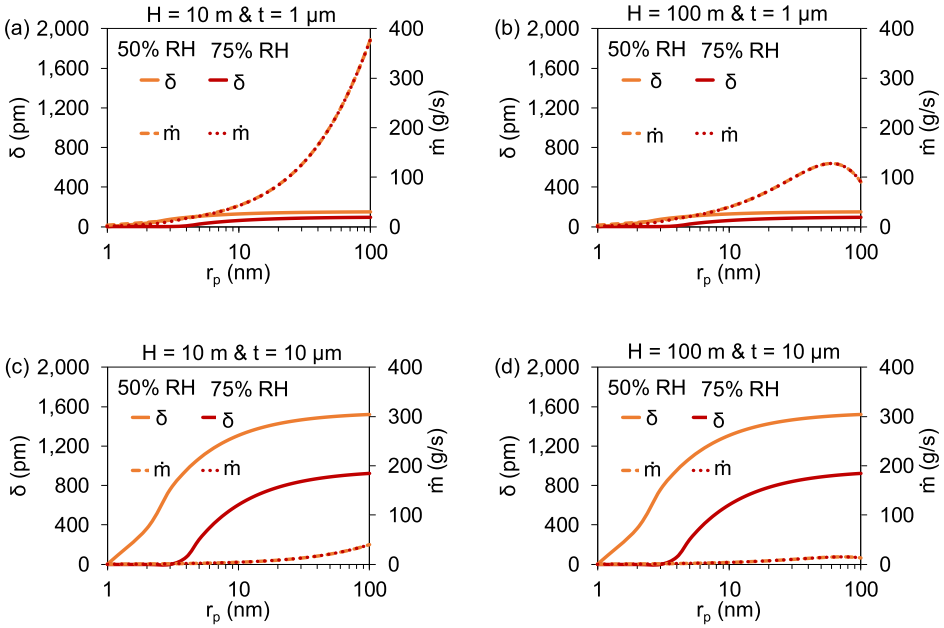

Fig. 12. Fig. 13 Graphs plotting the retreat distance (left y-axis) and transpiration rate (right y-axis) as functions of nanopore radius. These variables were calculated from Eqs. 1, 2, 3, 4, 5, and 6, where $\theta_R = 0^\circ$ and the ambient humidity was either 50% ($|P_K| = 95.1$ MPa) or 75% ($|P_K| = 39.5$ MPa). The tube height and leaf thickness were: (a) 10 m and 1 μm, (b) 100 m and 1 μm, (c) 10 m and 10 μm, or (d) 100 m and 10 μm.

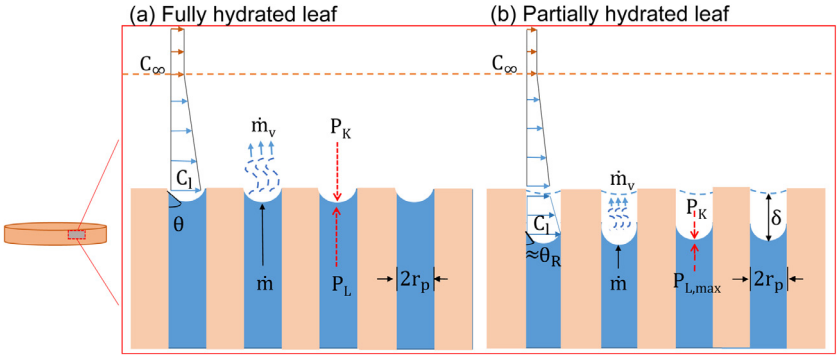

Fig. 13. Schematic of a synthetic leaf in a non-uniform humidity environment, where a diffusive concentration boundary layer exists above the leaf. (a) When the Laplace suction required to replenish water evaporating from the leaf is less than the maximum possible Laplace pressure ($|P_K| = |P_L| < |P_{L,max}|$), the menisci are stabilized along the outer face of the synthetic leaf. (b) When the evaporation rate exceeds a critical value, conservation of mass requires a Laplace pressure that exceeds what is possible ($|P_K| > |P_{L,max}|$). In this case, the menisci recede until achieving a reduced evaporation rate and increased local vapor concentration (c_l) where mass is conserved and $P_K \approx P_{L,max}$.

angle and nanopore radius. For the 1 nm pore size, where there is a regime of zero retreat, the ambient water activity sets the lower limit for the local water activity. For the 10 and 100 nm pore radii, where the menisci are always in the retreat regime, the local water activity varies continuously and is always higher than the ambient water activity. The local water activity approaches unity (regardless of the ambient humidity) as the receding contact angle increases to 89°, as the maximum Laplace suction approaches zero.

Fig. 12 shows how varying the tree geometry affects the retreat distance (left y-axis) and maximum possible transpiration rate (right y-axis). As shown earlier, the menisci will retreat into the nanopores when the ambient humidity results in a Kelvin stress that is greater than the maximum possible Laplace pressure the pores can sustain. The extent of retreat, calculated from Eq. 5, initially increases rapidly with increasing pore radius and then approaches a plateau value around $r_p \approx 10$ nm. The retreat distance is always smaller for the 75% relative humidity compared to 50% for an equivalent tree geometry. Comparing Fig. 12 (a) to (b) and (c) to (d), increasing the tree height by a factor of ten doesn't change the extent of retreat, as the Kelvin pressure and maximum possible Laplace pressure are not dependent on the hydrostatic pressure. On the other hand, when comparing Fig. 12 (a) to (c) and (b) to (d), increasing the thickness by a factor of ten causes an equivalent increase in retreat distance, as evident algebraically in Eq. 5.

Fig. 12 shows that the transpiration rate increases by an order of magnitude when the pore size is increased by an order of magnitude. For $H = 10$ m trees, the Darcy pressure drop always dominates over the hydrostatic pressure, such that $\dot{m}_{max}$ increases monotonically with increasing r_p over the considered parameter space. For taller $H = 100$ m trees, $\dot{m}_{max}$ reaches a maximal value at a critical $r_p \approx 60$ nm, beyond which the hydrostatic penalty exceeds the benefit of increased leaf permeability. The magnitude of the $\dot{m}_{max}$ curves are smaller for $H = 100$ m compared to 10 m, due to the hydrostatic pressure removing a substantive portion of the suction that could be otherwise devoted to viscous flow. The $\dot{m}$ curves are identical for the 50% and 75% ambient humidities over the pressure-limited regime (i.e. when $\delta > 0$), which is the vast majority of the parameter space. However, beneath a critical value of r_p, the transpiration switches to the evaporation-limited regime. This cross-over happens at $r_{p,c} \approx 3$ nm for the 75% ambient humidity and $r_{p,c} \approx 1$ nm for the 50% ambient humidity, such that $\dot{m}$ is about twice as large for the 50% humidity case at $r_{p,c} \approx 1$ nm.

3.2. Non-uniform humidity environment

Up to this point, we assumed that water vapor emanating from the leaf was removed via a convective gas flow. Here, we now switch to the opposite case, where evaporation from the leaf is diffusive across a concentration boundary layer. In other words, even when the leaf is fully hydrated ($\delta = 0$), the local water activity will be higher than that in the far ambient ($a_l > a_\infty$). The most important consequence of the non-uniform humidity condition is that the Kelvin stress acting on the menisci, and by extension the matching Laplace pressure, are no longer directly prescribed by the ambient humidity. This also means that the transpiration rate is no longer prescribed by the ambient humidity either. Therefore, a new order of operations is required to be able to theoretically characterize the transpiration rate and negative pressure of the synthetic tree.

The water vapor concentration gradient immediately above the menisci ($\partial c/\partial z$) results in a diffusive flux governed by Fick's first law:

$$J_v = -D\frac{\partial c}{\partial z}, \tag{7}$$

where J_v is the evaporative flux and D is the diffusivity of water vapor in air. The exact value of $\partial c/\partial z$ is non-trivial to determine, as the overall concentration field between the meniscus and the far-field humidity is non-linear. If the temperature field, leaf geometry, and menisci shape are all known, one approach could be to numerically solve for the concentration field and the resulting evaporative flux.

The above approach, besides being complex to solve, is only valid at low heat fluxes where the flow is purely diffusive in nature. At higher heat fluxes, the bulk gas flow is additionally convective and Fick's law is no longer prescriptive [39]. In such cases, we can instead think of the problem in terms of heat transfer. Specifically, we estimate the evaporation mass flow rate by relating the amount of heat being captured by the synthetic leaf ($\dot{Q}$) to the latent heat of vaporization (L):

$$\dot{m}_v = \frac{\dot{Q}}{L}. \tag{8}$$

The source of $\dot{Q}$ could be solar, waste heat, or active heating elements; for the context of this theoretical study the exact heat source is irrelevant. The value of L varies weakly with temperature, here we arbitrarily assume a leaf temperature of 50 °C (reminiscent of existing solar steam generators under 1 sun irradiation [40]) such that $L \approx$ 2,382 kJ/kg.

By conservation of mass, at equilibrium the corresponding evaporation mass flow rate is equivalent to the liquid mass flow rate up the tree, such that:

$$\dot{m}_v = \dot{m} = \rho Q. \tag{9}$$

Conservation of mass is assured for the following reasons. The alternative scenario of $\dot{m}_v < \dot{m}$ is non-physical, as it would require the incompressible liquid water within the tree to become increasingly compressed. The opposite scenario of $\dot{m}_v > \dot{m}$ is also impossible to maintain, as the menisci contact angle would keep decreasing to increase the magnitude of the Laplace pressure until either $\dot{m}_v = \dot{m}$ is achieved or dryout occurs.

For a non-uniform humidity environment, conservation of mass is the only way to determine the magnitude of the Kelvin and Laplace pressures. Now that $\dot{m}$ is estimated by combining Eqs. 8 and 9, $Q = \dot{m}/\rho$ can be plugged into Eq. 3 to solve for P_L. If the solution yields $|P_L| < |P_{L,max}|$, the menisci do not need to retreat and will exhibit a contact angle determined by Eq. 2. The local water activity at the menisci can be calculated by equating Eqs. 1 and 2 and solving for a_l. Conversely, if $|P_L| > |P_{L,max}|$, the menisci are unstable and are forced to retreat until an equilibrium is achieved (i.e. $P_L = P_{L,max}$). The length of the retreat is still solved using Eq. 5, except now the value for P_K corresponds to the (unstable) local Laplace pressure ($|P_L| > |P_{L,max}|$) and is not linked to the ambient conditions.

In summary, theoretically characterizing transpiration for a non-uniform ambient necessitated an inversion in the order of operations. For the uniform humidity condition, the ambient imposed the local water activity, which was used to solve for the Laplace pressure and finally the transpiration rate. For the non-uniform ambient, on the other hand, we began with an evaporation rate imposed by the heat input, which was used to solve for the Laplace pressure and then finally the local humidity.

In Fig. 14(a), the relationship between the critical nanopore radius and the transpiration rate is shown. Each mass flow rate was plugged into Eq. 9 to solve for Q, which was then plugged into Eq. 3 to solve for the Laplace pressure that sustains the flow. The critical pore radius, corresponding to the maximum possible Laplace pressure, was obtained by equating Eq. 3 and Eq. 4 and numerically solving the resulting quadratic expression to give two roots of $r_{p,c}$ for the case of $\theta_R = 0°$. Finally, the root that obeys the physics of the hydraulics was chosen as the value of $r_{p,c}$. The multiple curves account for different choices in the tree height ($H =$ 10 m, 100 m, or 1,000 m) and leaf thickness ($t =$ 1 μm or 10 μm).

The curves illustrate that the critical pore size decreases as the transpiration rate increases, because the corresponding increase in the Darcy and Poiseuille pressures requires a larger suction (i.e. Laplace) pressure. For a given transpiration rate and leaf thickness, increasing the tree height causes an almost-linear decrease in the critical pore radius. This is because the hydrostatic pressure, and to a lesser extent the viscous Poiseuille losses in the tubes, are increasing while the Darcy pressure drop stays the same. The change in tree height has a dramatic effect on $r_{p,c}$ for both thin and thick leaves, where the hydrostatic pressure can overwhelm the Darcy pressure. For example, for a $t =$ 1 μm leaf, $r_{p,c}$ decreases by an order of magnitude when changing $H =$ 10 m ($r_{p,c} \approx$ 1,455 nm) to $H =$ 100 m ($r_{p,c} \approx$ 145 nm), and $r_{p,c}$ decreases by two orders of magnitude when changing $H =$ 10 m ($r_{p,c} \approx$ 1,455 nm) to $H =$ 1,000 m ($r_{p,c} \approx$ 14 nm). Similarly, for a $t =$ 10 μm leaf, $r_{p,c}$ decreases by an order of magnitude when changing $H =$ 10 m ($r_{p,c} \approx$ 1,446 nm) to $H =$ 100 m ($r_{p,c} \approx$ 135 nm), and here we noticed that the whole transpiration rate range considered cannot be sustained when changing to $H =$ 1,000 m. In this special case of $t =$ 10 μm and $H =$ 1,000 m, the product of an increase in both the viscous and hydrostatic pressures drops results in an unsustainable suction pressure. In contrast, changing the leaf thickness for a fixed height does not dramatically change the critical pore size at very small flow rates, but as the transpiration rate is increased the thicker leaf is observed to exhibit a faster cut off point where flow can no longer be sustained due to the increase in the associated Darcy pressure drop. This is seen for a $H =$ 10 m, where the $t =$ 1 μm leaf can sustain flow for the whole transpiration rate range considered, while the $t =$ 10 μm leaf has a flow cut off point of $\dot{m} =$ 0.25 kg/s. Similarly, for the $H =$ 100 m tall tree, the $t =$ 1 μm sustains an increasing transpiration rate up to $\dot{m} =$ 0.25 kg/s but a thicker leaf of $t =$ 10 μm could only sustain an increased flow rate until $\dot{m} =$ 0.034 kg/s. The $H =$ 1,000 m tall and $t =$ 1 μm thick leaf tree could sustain a flow rate up to $\dot{m} =$ 0.034 kg/s but as explained above the $H =$ 1,000 m tall and $t =$ 10 μm thick leaf combines to form a suction pressure too much for the tree to sustain. The area beneath each curve corresponds to the evaporation-limited regime, where the Laplace pressure is less than the maximum value. The curves themselves represent the largest possible pore size to sustain a given flow rate, where the maximum Laplace pressure is required. In other words, the curves

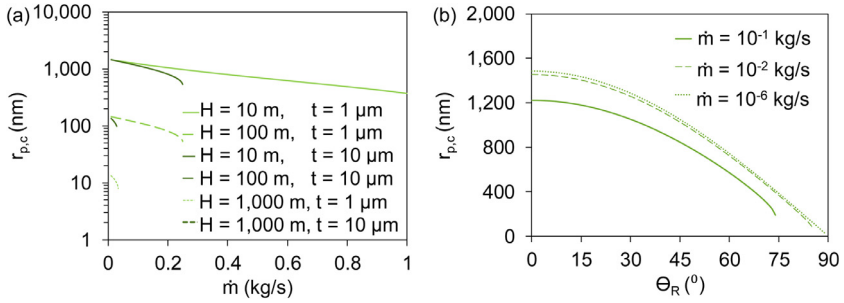

Fig. 14. (a) Graph of the critical nanopore size as a function of the transpiration rate, for six different tree geometries. Curves were obtained by combining Eqs. 3 and 4 and solving for the second of two roots from the resulting quadratic expression. Curves extend across the evaporation-limited regime, coming to a halt at the pressure-limited regime where $\dot{m}=\dot{m}_{max}$. (b) The critical pore radius is graphed as a function of the nanopore's receding contact angle, for three fixed choices of transpiration rate. The tube height was $H=$ 10 m and the leaf thickness was $t=$ 1 μm).

themselves represent the pressure-limited regime, while the phase space above the curves is not obtainable.

No longer assuming a fixed $\theta_R=0^\circ$, in Fig. 14(b) $r_{p,c}$ is plotted against θ_R for three different transpiration rates. The numerical scheme to solve for $r_{p,c}$ is the same as that already discussed for Fig. 14(a). Increasing θ_R decreases the maximum Laplace pressure possible for a given nanopore radius, which explains the corresponding non-linear decrease in $r_{p,c}$ required to sustain a given transpiration rate. For example, increasing the receding contact angle by a factor of four from 15° to 60° reduces the critical pore size by about a factor of at least 1.9. The curves also reveal that increasing $\dot{m}$ results in a disproportionate decrease in $r_{p,c}$ for any given θ_R, for example $r_{p,c}$ increases from 1,223 nm to 1,454 nm for an order of magnitude decrease in $\dot{m}$ and increases from 1,223 nm to 1,484 nm for five orders of magnitude decrease in $\dot{m}$, and in both cases $\theta_R=0^\circ$.

Fig. 15 illustrates how the suction pressure requirement can vary widely as the transpiration rate is continuously varied from $\dot{m}=$ 0–20 g/s. In each graph, the required Laplace pressure is plotted against the transpiration rate, with each curve coming to an abrupt halt if reaching $\dot{m}_{max}$ (and the corresponding $P_{L,max}$). Each of the six graphs depicts a different combination of tree heights and leaf thicknesses, with the three data series in turn representing different choices in nanopore radius. The general trend is that, as $\dot{m}$ increases, the hydrostatic pressure remains fixed while the Darcy and Poiseuille pressure drops increase. This increases the suction requirement, hence the increase in P_L. For example, increasing $r_{p,c}$ by a factor of 10 for any given transpiration rate causes a reduction of the Darcy pressure drop by a factor of 100.

Fig. 15(a) shows that for a 10 m tall tree with a leaf thickness of $t=1$ μm, transpiration is possible over the full range of $\dot{m}=$ 0–20 g/s flow rates for the moderate ($r_p=$ 10 nm) and large (100 nm) nanopores. For the $r_p=$ 1 nm case, on the other hand, the massive Darcy pressure drop resulted in a maximal transpiration rate of only $\dot{m}_{max}=$ 4.3 g/s. The $r_p=$ 1 nm tree exhibited the largest maximum suction pressure of $|P_{L,max}|=$ 145.6 MPa, which may seem counter-intuitive considering it exhibits the smallest range of transpiration rates. However, as discussed in the previous section, the proportionate increase in P_L with decreasing r_p is always more than offset by the non-linear increase in Darcy pressure.

In Fig. 15(b), the tree was made taller ($H=$ 100 m) while retaining a leaf thickness of $t=1$ μm. The resulting increase in the hydrostatic and Poiseuille pressure drops has a noticeable effect on the required suction pressure for the $r_p=$ 10 nm and 100 nm leaves. Specifically, the pressure curves are shifted upward by about an order of magnitude, while the slope of the curves becomes weaker especially for the $r_p=$ 100 nm case where the curve is virtually flat. This is because the hydrostatic pressure becomes entirely dominant for $r_p=$ 100 nm and appreciable for $r_p=$ 10 nm, relative to the Darcy pressure. However, in both cases, transpiration was still possible over the entire range of considered flow rates ($\dot{m}=$ 0–20 g/s). The curve for the $r_p=$ 1 nm leaf is essentially unchanged from Fig. 15(a). This is because the Darcy pressure ranges from $P_D\sim$ 10–100 MPa at appreciable flow rates, which overwhelms even the increased hydrostatic pressure of 0.98 MPa.

When increasing the tree height still further to $H=$ 1,000 m in Fig. 15(c), even the maximal Laplace pressure (- 1.45 MPa) of the $r_p=$ 100 nm leaf can no longer hold the water columns against gravity (9.8 MPa). For the $r_p=$ 10 nm leaf, the pressure curve is shifted upward by another order of magnitude with its slope flattened even more. The full range of transpiration rates can no longer be sustained, with a maximum flow rate of 13.3 g/s. This is still superior to the $r_p=$ 1 nm leaf, which reaches its maximum Laplace pressure at a flow rate of only 4.0 g/s. These findings indicate that the optimal choice for nanopore size tends to correspond to the largest possible value, as long as it still readily overcomes the hydrostatic pressure requirement.

Comparing Fig. 15(a) and (d), we see the effect of making the leaf thicker while keeping the height constant for the three pore radii considered. A thicker leaf increases the contribution of the Darcy pressure drop to the suction pressure at any given transpiration rate, such that increasing the leaf thickness by a factor of 10 causes the maximum sustainable Laplace pressure to be reached at a transpiration rate of only 0.5 g/s for the 1 nm pore radius, as opposed to 4.3 g/s in Fig. 15(a). The increase in the viscous pressure drop causes the maximum Laplace pressure to be reached at a transpiration rate of 4.3 g/s for the 10 nm pore radius, whereas for the thinner leaf in Fig. 15(a) the flow was sustained through the range plotted. For $r_p=$ 100 nm, the large permeability mitigates the increased viscous effect and transpiration was still possible across the considered range of $\dot{m}=$ 0–20 g/s. Figs. 15(e) and (f) similarly increase the leaf thickness to $t=$ 10 μm while exhibiting the same tree height as Figs. 15(b) and (c), respectively. An analogous trend is observed, where the pressure curves shift upward and therefore terminate at an earlier $\dot{m}_{max}$, especially for the smaller pore sizes which are most sensitive to the Darcy pressure.

Fig. 16 plots the transpiration rate and menisci retreat distance (if any), as a function of the heat being absorbed by the synthetic leaf. The four graphs vary the tree height ($H=$ 10 m and 100 m) and leaf thickness ($t=$ 1 μ m and 10 μ m) while fixing the nanopore radius at $r_p=$ 1 nm. The transpiration rate was calculated using Eq. 8 and increases linearly with $\dot{Q}$, until reaching a plateau value of $\dot{m}_{max}$ that corresponds to the maximum possible suction pressure ($P_{L,max}$). Any further increase in $\dot{Q}$ cannot increase the flow rate, as the tree has crossed over from the evaporation-limited (i.e. heat-limited) regime to the pressure-limited regime.

For Fig. 16 a ($H=$ 10 m and $t=$ 1 μ m), the maximum transpiration rate of $\dot{m}=$ 4.28 g/s is reached at a critical heater power of

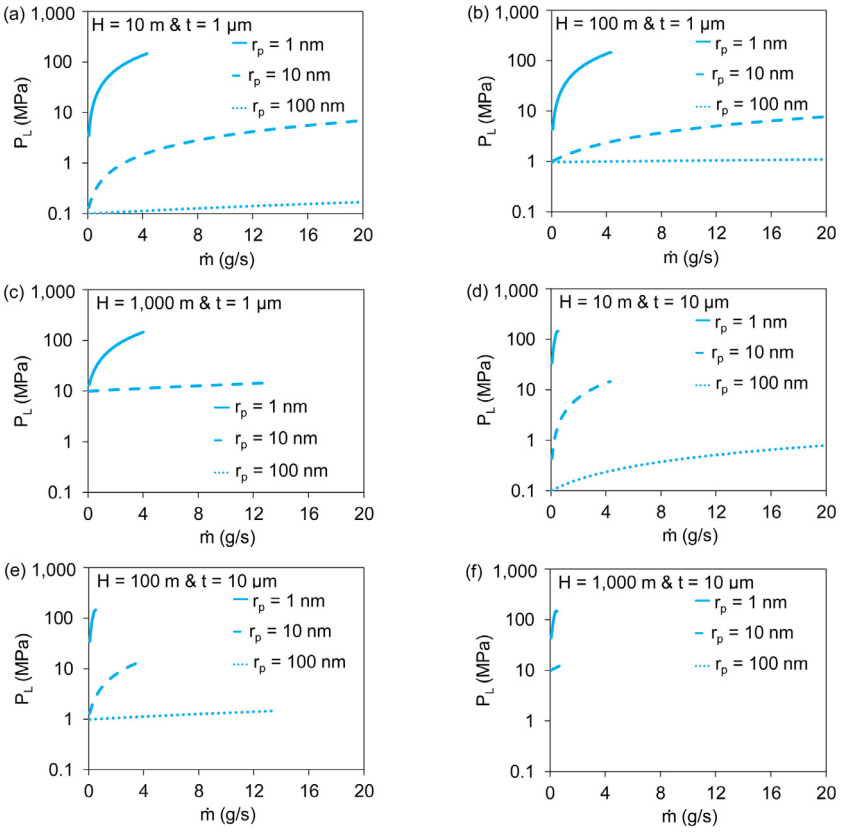

Fig. 15. (a–f) Laplace pressure versus the transpiration rate for 18 different tree geometries. This suction pressure is calculated from summing up the pressure drops across the synthetic tree (Eq. 3) to achieve any given flow rate. The transition from the evaporation-limited to pressure-limited regimes occurs at the end of each curve, where the value of $\dot{m}_{max}$ depended on the tree geometry.

$\dot{Q}_c = 10.20$ kW. These numbers are approximately the same when the tree height is increased from $H = 10$ m to $H = 100$ m (Fig. 16 b), due to the overwhelming dominance of the Darcy pressure drop when $r_p = 1$ nm, as explained earlier. In Figs. 16 (c) and (d), increasing the leaf thickness (and Darcy pressure) by a factor of 10 results in a 10-fold decrease in the maximal transpiration rate ($\dot{m} = 0.428$ g/s). The heater power at which this crossover occurs is also reduced by an order of magnitude, to $\dot{Q}_c = 1.02$ kW.

For all four curves, the retreat distance is initially zero because maximum Laplace pressure has not yet been reached. For heater powers that exceed the critical value ($\dot{Q} > \dot{Q}_c$), the evaporation mass flow rate can no longer be matched by even the maximal liquid mass flow rate. Therefore, the menisci must retreat until reaching equilibrium. The retreat distance is calculated by solving for the (unattainable) suction pressure value that would conserve mass Eqs. 3 and (8) and plugging it into Eq. 5 as P_K, i.e. the equivalent local Kelvin pressure acting on the menisci. Finally, Eq. 5 is solved for the retreat distance δ where equilibrium is achieved at a flow rate corresponding to $P_{L,max}$. Intuitively, the retreat distance increases (non-linearly) with increasing values of $\dot{Q} > \dot{Q}_c$. The extent of retreat is nearly independent of the tree height but greatly affected by the thickness of the leaves. For example, for $\dot{Q} = 12$ kW the retreat is $\delta \sim 27$ pm when $t = 1$ μ m, compared to $\delta \sim 16$ nm when $t = 10$ μ m. Note that this approach assumes that, as the menisci retreat, an increasing portion of the heat input to the leaf will no longer be used for pure evaporation. In cases where this assumption is not valid (i.e. all heat must be used for evaporation), the leaf would simply dry out for heat values exceeding $\dot{Q}_c$ instead of maintaining $\dot{m}_{max}$.

Fig. 17 is equivalent to Fig. 16, but with a larger fixed nanopore radius of $r_p = 10$ nm. For Fig. 17 a ($H = 10$ m and $t = 1$ μ m), the maximum transpiration rate was never reached for the considered range of $\dot{Q}_c = 1 - 12$ kW, such that the leaf always remained fully hydrated. This was also observed when increasing the tree height from $H = 10$ m to $H = 100$ m (Fig. 17 b). In other words, the Darcy pressure drop is still dominant over gravity, but at the same time is reduced substantively relative to the $r_p = 1$ nm tree to avoid the pressure-limited regime. In Figs. 17 (c) and (d), the increased leaf thickness (and Darcy pressure) resulted in a maximum transpiration rate of $\dot{m} = 4.26$ g/s at $\dot{Q}_c = 10.12$ kW for the $H = 10$ m tall tree, and $\dot{m} = 4.0$ g/s reached at $\dot{Q}_c = 9.52$ kW for the $H = 100$ m tall tree. The taller tree switched to the pressure-limited regime at a slightly smaller critical heat input, due to its more appreciable hydrostatic pressure drop reducing the pressure available for viscous flow. As in Fig. 16, the retreat distance increased non-linearly with $\dot{Q} > \dot{Q}_c$, with $\delta \sim 10$ pm for the $r_p = 10$ nm and $t = 10$ μm tree being comparable to the prior case of $r_p = 1$ nm and $t = 1$ μ m.

Fig. 18 continuously varies the nanopore radius to show how it affects the local water activity (left y-axis) that corresponds to the maximum possible transpiration rate (right y-axis). For a non-uniform humidity environment, the water activity at the menisci is not initially known and differs from the far ambient value. Each value of r_p is plugged into Eq. 4, setting $\theta_R = 0^\circ$ to get the corresponding maximum pressure, equating this to 1, and finally solving for a_l. Increasing the pore size resulted in increased water activities, which is intuitive because the smaller magnitude of the Laplace and Kelvin pressures necessitates a higher local humidity. The four curves of a_l versus r_p in Figs. 18 (a)–(d) are identical, as a_l is independent of the tube height and leaf thickness.

Conversely, the maximum transpiration rate is strongly dependent on these variables, as they affect the hydrostatic and viscous pressure drops that determine the flow rate (Eq. 3). For the

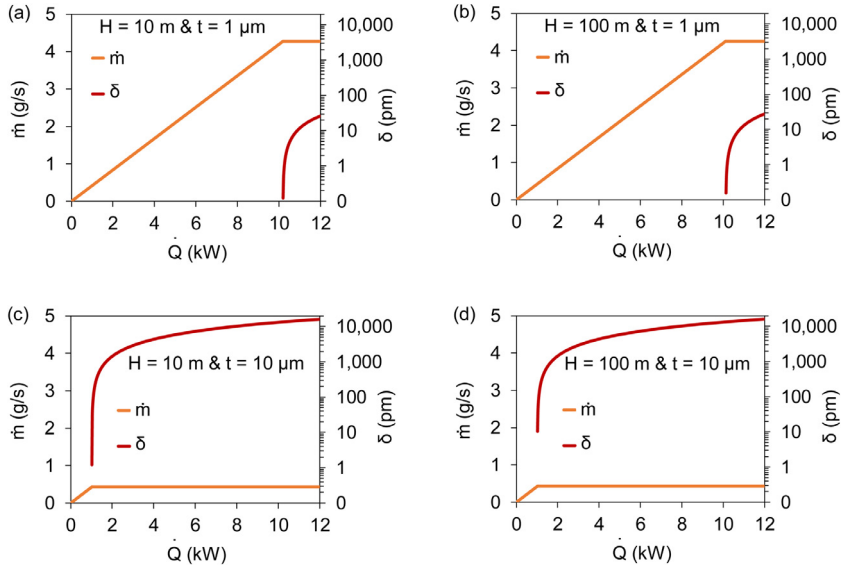

Fig. 16. (a–d) The transpiration rate (left y-axis) and retreat distance (right y-axis) as functions of applied heater power for various H and t and fixed $r_p = 1$ nm. Values for $\dot{m}$ were obtained by solving Eqs. 3, 8, and 9, where the curves plateaued when the associated Laplace pressure became maximal (i.e. pressure-limited regime). Menisci retreat, exclusive to the pressure-limited regime, was determined from Eq. 5 using an average linear conductance ratio of $\beta = 1.49 \times 10^{-4}$ corresponding to $r_p = 1$ nm.

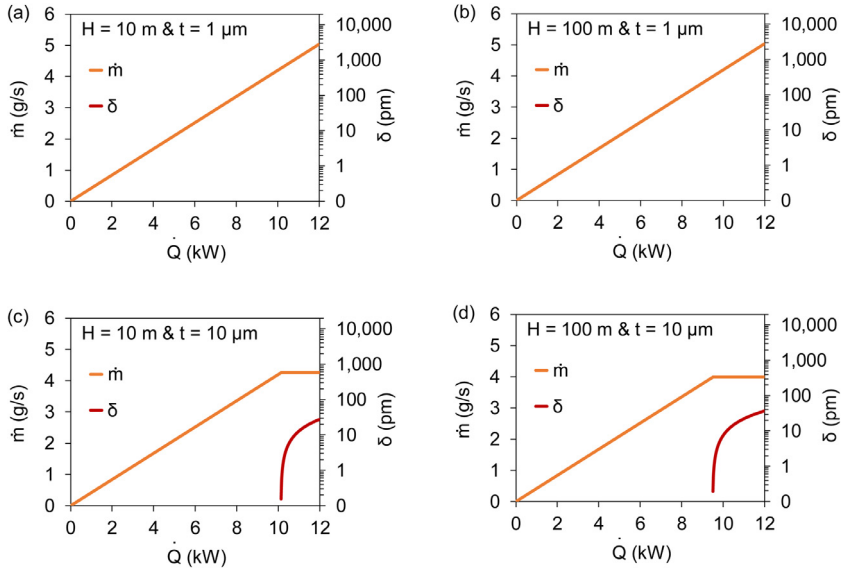

Fig. 17. Equivalent graphs to Fig. 16, but with $r_p = 10$ nm (and $\beta = 1.49 \times 10^{-5}$) instead of $r_p = 1$ nm. In this case, only (c) and (d) exhibit the pressure-limited regime and menisci retreat over the range of heat inputs considered.

short trees, Fig. 18(a) and (c), the maximum transpiration rate increases monotonically with r_p due to the decrease in the dominant Darcy pressure drop. For the taller trees, Fig. 18(b) and (d), the $\dot{m}_{max}$ curves reach a maximum at $r_{p,c} \approx 62$ nm for $t = 1$ μ m and $r_{p,c} \approx 72$ nm for $t = 10$ μ m. Beyond these peaks, the benefit of decreasing the Darcy pressure with increasing r_p is no longer worth the decrease in $|P_{L,max}|$. Beyond the range of values shown here, these curves will eventually drop to $\dot{m}_{max} \to 0$, once the entire maximum Laplace pressure is consumed by the hydrostatic pressure in the tubes. Considering that water at the menisci must be evaporating to sustain transpiration, an important constraint is $a_l > a_\infty$ for the concentration boundary layer above the leaf. This breaks down beneath $r_p = 1$ nm for $a_\infty = 0.5$ and beneath $r_p = 3$ nm for $a_\infty = 0.75$, such that $\dot{m}_{max} \to 0$. In other words, at a sufficiently small nanopore radius, the maximum Laplace pressure is not achievable because its corresponding Kelvin pressure would preclude the possibility of evaporation. Of course, smaller flow rates where $|P_L| < |P_{L,max}|$ are still possible, as these occur at larger local water activities.

Fig. 19 similarly plots the local water activity and maximum transpiration rate, but now for varying receding contact angles and a fixed $r_p = 1$ nm. Increasing θ_R increases the minimum possible radius of curvature, which decreases the magnitude of the maximum possible Laplace and Kelvin pressures. This results in the trend of an increased a_l (corresponding to the maximum transpiration rate) with increasing θ_R. Changing the tube height from $H = 10$ m to 100 m did not change the shape of the $\dot{m}_{max}$ curves, due to the preeminence of the Darcy pressure. Changing the leaf thickness decreased the $\dot{m}_{max}$ curves by about an order of magnitude. Analogous with the previous figure, these curves abruptly terminated beneath a critical receding contact angle where the menisci became saturated with respect to the ambient humidity. This crossover from evaporation to condensation for menisci at the

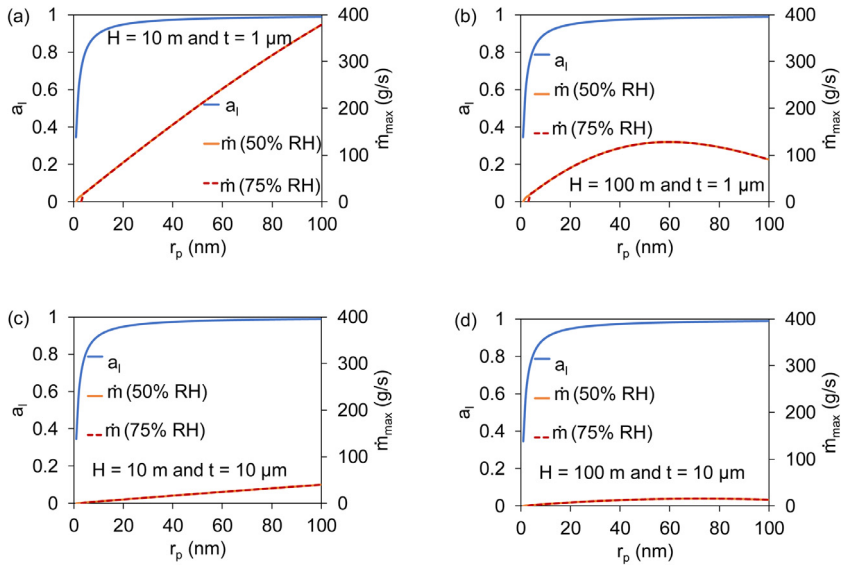

Fig. 18. Graphs plotting the local water activity (left y-axis) and maximum transpiration rate (right y-axis) as functions of nanopore radius. These variables are calculated from Eqs. 1, 3, 4, and 9 for $\theta_R = 0^\circ$, varying β (Eq. 6), and ambient humidities of either 50% or 75%. The tree geometry was varied as: (a) $H = 10$ m and $t = 1$ μm, (b) $H = 100$ m and $t = 1$ μm, (c) $H = 10$ m and $t = 10$ μm, and (d) $H = 100$ m and $t = 10$ μm. Note that $\dot{m}_{max}$ corresponding to the maximum Laplace pressure is not possible beneath a critical r_p where the local humidity matches the ambient one.

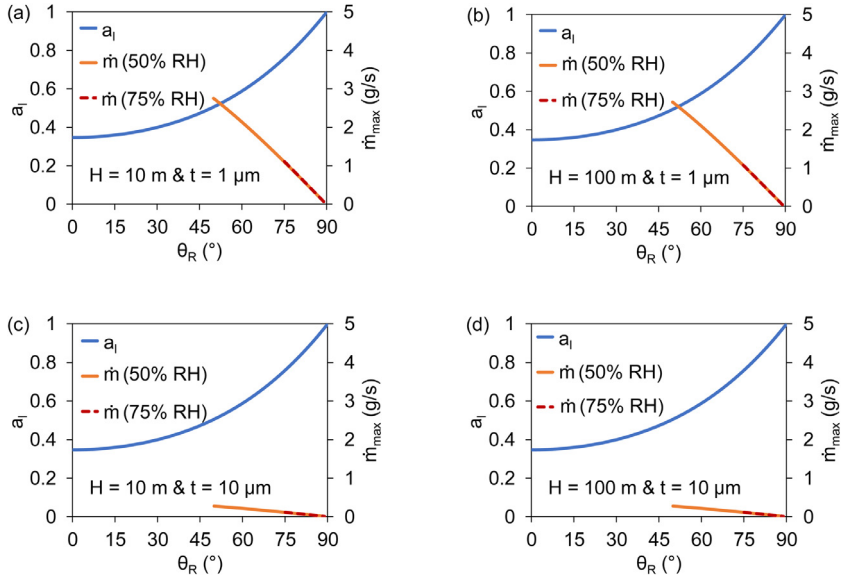

Fig. 19. Plots of the local water activity (left y-axis) and maximum transpiration rate (right y-axis) as functions of the receding contact angle. Curves are calculated from a combination of Eqs. 2, Eq. 3, Eq. 9 and Eq. 1 for $r_p = 1$ nm and an ambient humidity of either 50% or 70%. The different graphs correspond to tree geometries of: (a) $H = 10$ m and $t = 1$ μm, (b) $H = 100$ m and $t = 1$ μm, (c) $H = 10$ m and $t = 10$ μm, and (d) $H = 100$ m and $t = 10$ μm.

maximum Laplace pressure occurred at $\theta_R < 50^\circ$ for $a_\infty = 0.5$ and $\theta_R < 75^\circ$ for $a_\infty = 0.75$.

4. Conclusions

We analytically modeled the stability and transpiration rate of synthetic trees across a wide variety of tree geometries and environmental conditions. Our model tree system was comprised of an upper nanoporous film that was connected to an array of vertically-oriented tubes of millimetric diameter. In particular, we found that whether or not a diffusive diffusive boundary layer exists above the synthetic leaf dramatically affects the physics of the transpiration process as summarized visually in Fig. 20. Applying our model over a wide parameter space, the following advances were made regarding our understanding of transpiration in synthetic trees:

(i) Experimental reports of synthetic trees have alternately used a dry gas flow to result in a negligible boundary layer over the leaf [3,20–23], or a natural ambient with a diffusive boundary layer [26–29,31]. In hindsight, these two approaches result in fundamentally distinct physics for the resulting transpiration, which was not properly appreciated and contextualized until the present work.

(ii) The stresses acting on the evaporating water menisci within a synthetic leaf vary depending on the environmental conditions. In the absence of an appreciable diffusive boundary layer, the controlled ambient humidity is equivalent to the local humidity just above a fully hydrated leaf. For this reason, the ambient humidity directly prescribes the Kelvin and Laplace pressures acting on the menisci. In contrast, in the presence of a diffusive boundary layer,

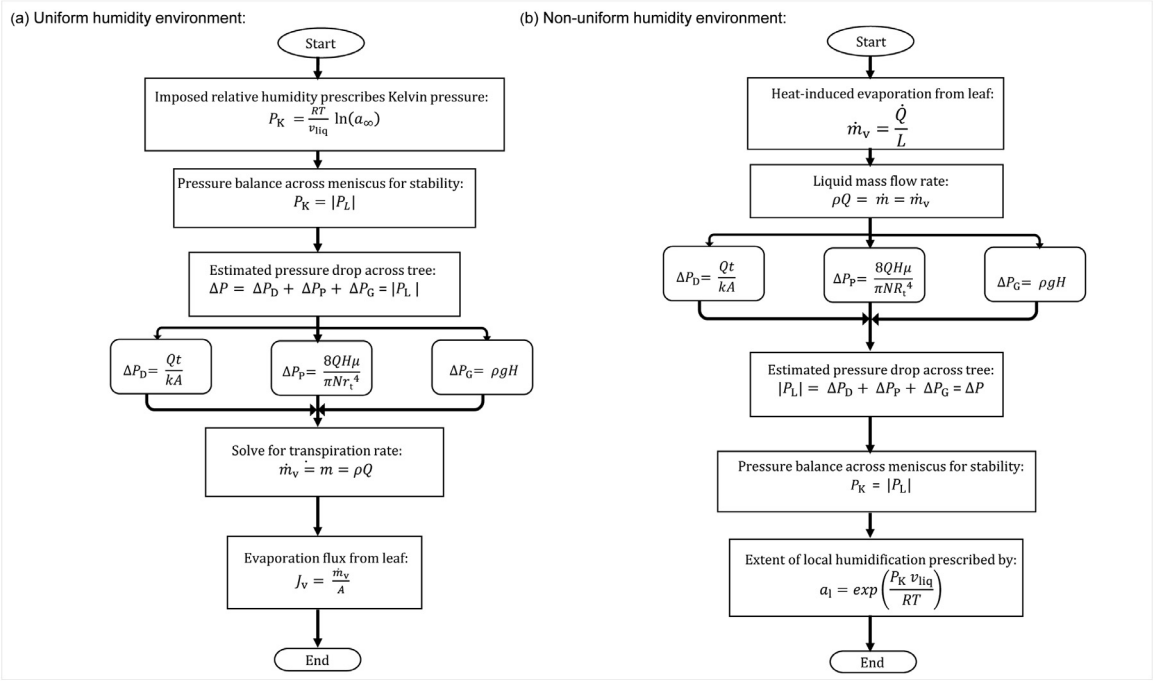

Fig. 20. Order of operations for modeling a synthetic tree's hydraulics for a: **(a)** Uniform humidity environment, or **(b)** Non-uniform humidity environment.

the local humidity is higher than that of the ambient and is not known *a priori*. Therefore, the Kelvin and Laplace pressures at the menisci must instead be determined by measuring and/or controlling the liquid flow rate across the tree and back calculating the associated suction pressure.

(iii) The steady-state transpiration rate is a dual function of the Laplace pressure generated within the leaf, which defines the sum of the pressure drops across the tree, and the tree's geometry, which tunes the water's flow rate for a given pressure drop. For relatively short synthetic trees ($H \lesssim 10$ m), the viscous pressure drop across the leaf is dominant over the hydrostatic and Poiseuille pressure drops across the vertical tubes. Therefore, the transpiration rate can be increased monotonically by increasing the radius (i.e. permeability) of the leaf's nanopores. To date, reports on synthetic trees have tended to emphasize minimizing the nanopore size to maximize the Laplace suction [20,25], but our finding indicates that for short trees it is actually the larger nanopores with weaker suction that result in the most effective transpiration. This is because the Darcy pressure is inverse to the square of the nanopore radius, whereas the Laplace suction is merely inverse to the nanopore radius. In contrast, for tall synthetic trees of order $H \sim$ 100–1,000 m, the hydrostatic pressure can dominate over the Darcy pressure under most flow conditions. In this case, decreasing the nanopore radius results in a higher transpiration rate, as the increased Laplace suction better overcomes the fixed hydrostatic load.

(iv) When the Laplace pressure is beneath its maximal possible value, the transpiration rate is evaporation-limited. In this regime, the Laplace pressure and transpiration rate can be tuned over a wide range of values by varying the ambient humidity (for a uniform humidity environment) or by varying the heat input to the leaf (for a non-uniform humidity environment). When the maximum Laplace pressure is reached, the transpiration rate is now maximal and fixed, which we call the pressure-limited regime. The cross-over between the evaporation-limited and pressure-limited regimes depends purely upon the ambient humidity and nanopore radius for a pure vapor environment. For a non-uniform humidity environment, the cross-over instead depends on the evaporation rate (i.e. heat input to the leaf) and the geometry of the entire tree, which defines what suction is required for the liquid mass flow rate to balance the evaporative mass flow rate.

(v) In a uniform humidity environment, the leaf is fully hydrated when the ambient humidity is above a critical value that depends on the nanopore radius. Beneath this critical value, the Kelvin pressure imposed on the menisci exceeds the maximum possible Laplace suction that can be sustained, such that the menisci retreat within the leaf. Due to the evaporative vapor getting choked within the dried-out nanopores, the local humidity increases until reaching a retreat distance where the Kelvin stress now matches the maximum Laplace pressure. Conversely, in a non-uniform humidity environment, the menisci are shielded by a diffusive boundary layer such that the ambient environment does not dictate the local Kelvin stress or when the menisci retreat. Instead, retreat would only occur when the heat input to the leaf corresponds to an evaporation rate that exceeds a critical value. Beyond this critical evaporation rate, even the maximum possible Laplace pressure cannot preserve leaf hydration, such that the menisci must retreat until the evaporation rate is decreased.

We hope that this model and discussions will help the future development of sophisticated and stable synthetic trees, whose capillary-induced hydraulics show much promise for various applications in water harvesting, energy harvesting, and phase-change heat transfer systems.

Declaration of Competing Interest

The authors declare that they have no known competing financial interests or personal relationships that could have appeared to influence the work reported in this paper.

CRediT authorship contribution statement

Ndidi L. Eyegheleme: Conceptualization, Methodology, Validation, Formal analysis, Writing – original draft, Visualization. **Kurt Peng:** Methodology, Validation, Writing – review & editing.

Jonathan B. Boreyko: Conceptualization, Methodology, Writing – review & editing, Supervision, Funding acquisition.

Acknowledgments

This work was supported by a National Science Foundation CAREER Award (CBET-1653631).

References

[1] G.W. Koch, S.C. Sillet, G.M. Jennings, S.D. Davis, The limits to tree height, Nature 428 (2004) 851–854.
[2] N.M. Holbrook, M.A. Zwieniecki, Vascular transport in plants, Academic Press, 2011.
[3] A.D. Stroock, V.V. Pagay, M.A. Zwieniecki, N.M. Holbrook, The physicochemical hydrodynamics of vascular plants, Annu. Rev. Fluid Mech. 46 (2014) 615–642.
[4] P.F. Scholander, How mangroves desalinate seawater, Physiol. Plant 21 (1968) 251–261.
[5] A.K. Parida, B. Jha, Salt tolerance mechanisms in mangroves: a review, Trees 24 (2010) 199–217.
[6] I. Paudel, A. Naor, Y. Gal, S. Cohen, Simulating nectarine tree transpiration and dynamic water storage from responses of leaf conductance to light and sap flow to stem water potential and vapor pressure deficit, Tree Physiol 35 (2015) 425–438.
[7] K. Kim, E. Seo, S.K. Chang, T.J. Park, S.J. Lee, Novel water filtration of saline water in the outermost layer of mangrove roots, Sci. Rep. 6 (2016) 20426.
[8] K.A. Novick, C.F. Miniat, J.M. Vose, Drought limitations to leaf-level gas exchange: results from a model linking stomatal optimization and cohesion-tension theory, Plant Cell Environ 39 (2016) 583–596.
[9] H.J. Schenk, S. Espino, D.M. Romo, N. Nima, A.Y.T. Do, J.M. Michaud, B. Papahadjopoulos–Sternberg, J. Yang, Y.Y. Zuo, K. Steppe, S. Jansen, Xylem surfactants introduce a new element to the cohesion–tension theory, Plant Physiol (2016) 1–41.
[10] F. Bentrup, Water ascent in trees and lianas: the cohesion-tension theory revisited in the wake of Otto Renner, Protoplasma 254 (2017) 627–633.
[11] F. Lens, A. Tixier, H. Cochard, J.S. Sperry, S. Jansen, S. Herbette, Embolism resistance as a key mechanism to understand adaptive plant strategies, Curr. Opin. Plant Biol. 16 (2013) 287–292.
[12] F. Caupin, A. Arvengas, K. Davitt. M. E. M. Azouzi, K.I. Shmulovich, C. Ramboz, D.A. Sessoms, A.D. Stroock, Exploring water and other liquids at negative pressure, J. Phys. Condens. Matter 24 (2012) 284110.
[13] H.R. Brown, The theory of the rise of sap in trees: some historical and conceptual remarks, Phys. Perspect. 15 (2013) 320–358.
[14] J. Cai, M.T. Tyree, Measuring vessel length in vascular plants: can we divine the truth? History, theory, methods, and contrasting models, Trees 28 (2014) 643–655.
[15] G. Petit, A. Crivellaro, Comparative axial widening of phloem and xylem conduits in small woody plants, Trees 28 (2014) 915–921.
[16] H.K. Kim, J. Park, I. Hwang, Investigating water transport through the xylem network in vascular plants, J. Exp. Bot. 65 (2014) 1895–1904.
[17] H.H. Dixon, J. Joly, On the ascent of sap, Philos. Trans. R. Soc. B 186 (1895) 563–576.
[18] H.F. Thut, Demonstration of the lifting power of evaporation, Ohio J. Sci. 28 (1928) 292–298.
[19] A.T.J. Hayward, Mechanical pump with a suction lift of 17 metres, Nature 225 (1970) 376–377.
[20] T.D. Wheeler, A.D. Stroock, The transpiration of water at negative pressures in a synthetic tree, Nature 455 (2008) 208–212.
[21] X. Noblin, L. Mahadevan, I.A. Coomaraswamy, D.A. Weitz, N.M. Holbrook, M.A. Zwienieck, Optimal vein density in artificial and real leaves, Proc. Natl. Acad. Sci. U.S.A. 105 (2008) 9140–9144.
[22] O. Vincent, D.A. Sessoms, E.J. Huber, J. Guioth, A.D. Stroock, Drying by cavitation and poroelastic relaxations in porous media with macroscopic pores connected by nanoscale throats, Phys. Rev. Lett. 113 (2014) 134501.
[23] V. Pagay, M. Santiago, D.A. Sessoms, E.J. Huber, O. Vincent, A. Pharkya, T.N. Corso, A.N. Lakso, A.D. Stroock, A microtensiometer capable of measuring water potentials below $-$10 {M}{P}a, Lab Chip 14 (2014) 2806–2817.
[24] R.L. Agapov, J.B. Boreyko, D.P. Briggs, B.R. Srijanto, S.T. Retterer, C.P. Collier, N.V. Lavrik, Length scale selects directionality of droplets on vibrating pillar ratchet, Adv. Mater. Interfaces 1 (2014) 1400337.
[25] O. Vincent, A. Szenicer, A.D. Stroock, Capillarity-driven flows at the continuum limit, Soft Matter 12 (2016) 6656–6661.
[26] M. Lee, H. Lim, J. Lee, Fabrication of artificial leaf to develop fluid pump driven by surface tension and evaporation, Sci. Rep. 7 (2017) 14735.
[27] O. Vincent, P. Marmottant, P.A. Quinto-Su, C.D. Ohl, Birth and growth of cavitation bubbles within water under tension confined in a simple synthetic tree, Phys. Rev. Lett. 108 (2012) 184502.
[28] C. Duan, R. Karnik, M.C. Lu, A. Majumdar, Evaporation-induced cavitation in nanofluidic channels, Proc. Natl. Acad. Sci. U.S.A. 109 (2012) 3688–3693.
[29] J. Li, C. Liu, Z. Xu, K. Zhang, X. Ke, L. Wang, A microfluidic pump/Valve inspired by xylem embolism and transpiration in plants, PLOS ONE 7 (2012) e50320.
[30] W. Shi, J.R. Vieitez, A.S. Berrier, M.W. Roseveare, D.A. Surinach, B.R. Srijanto, C.P. Collier, J.B. Boreyko, Self-stabilizing transpiration in synthetic leaves, ACS Appl. Mater. Interfaces 11 (2019) 13768–13776.
[31] W. Shi, R.M. Dalrymple, C.J. McKenny, D.S. Morrow, Z.T. Rashed, D.A. Surinach, J.B. Boreyko, Passive water ascent in a tall, scalable synthetic tree, Sci. Rep. 10 (2020) 230.
[32] N.L. Eyegheleme, W. Shi, L.H. De Koninck, J.L. O'Brien, J.B. Boreyko, Synthetic trees for enhanced solar evaporation and water harvesting, Appl. Phys. Lett. 118 (2021) 251601.
[33] L.M. Skinner, J.R. Sambles, The Kelvin equation–a review, J. Aerosol Sci. 3 (1972) 199–210.
[34] I.T. Chen, D.A. Sessoms, Z. Sherman, E. Choi, O. Vincent, A.D. Stroock, Stability limit of water by metastable vapor-liquid equilibrium with nanoporous silicon membranes, J. Phys. Chem. B 120 (2016) 5209–5222.
[35] S. Whitaker, Flow in porous media I: A theoretical derivation of Darcy's law, Transport Porous Med 1 (1986) 3–25.
[36] S. Gruener, D. Wallacher, S. Greulich, M. Busch, P. Huber, Hydraulic transport across hydrophilic and hydrophobic nanopores: Flow experiments with water and n-hexane, Phys. Rev. E 93 (2016) 013102.
[37] P.A. Crossley, L.M. Schwartz, J.R. Banavar, Image based models of porous media: Application to Vycor glass and carbonate rocks, Appl. Phys. Lett. 59 (1991) 3553–3555.
[38] I.R. Cowan, Stomatal Behaviour and Environment, Academic Press 4 (1978) 117–228.
[39] Z. Lu, K.L. Wilke, D.J. Preston, I. Kinefuchi, E. Chang-Davidson, E.N. Wang, An Ultrathin Nanoporous Membrane Evaporator, Nano Lett. 17 (2017) 6217–6220.
[40] H. Ghasemi, G. Ni, A.M. Marconnet, J. Loomis, S. Yerci, N. Miljkovic, G. Chen, Solar steam generation by heat localization, Nat. Commun. 5 (2014) 4449.